Transaction B: Mechanical Engineering
Vol. 16, No. 4, pp. 281–290

SCIENTIA IRANICA

Modeling of Twin-Entry Radial Turbine Performance Characteristics Based on Experimental Investigation Under Full and Partial Admission Conditions

A. Hajilouy[1,*], M. Rad[1] and M.R. Shahhosseini[1]

Abstract. *In this paper, the performance of a turbocharger twin-entry radial inflow turbine is investigated analytically and experimentally under steady state, full and partial admission conditions. In this modeling, the mass flow rate, pressure ratio and efficiency of the turbine are assumed unknown. The turbine geometry and the inlet total pressure and temperature are known, hence, the turbine performance characteristics can be obtained. In the turbocharger laboratory, performance characteristics of the turbine are determined, measuring the main parameters for various operating conditions. Comparing the model and experimental results shows good agreement. Also, considering the effect of test parameters on performance uncertainty, it shows that the pressure ratio has more influence. Finally, the uncertainty of efficiency decreases as the pressure ratio increases.*

Keywords: *Radial inflow turbine; Full and partial admission conditions; Modeling; Turbocharger.*

INTRODUCTION

Radial inflow turbines are widely used in diesel and CNG engine turbochargers, increasing power and efficiency and decreasing SFC in engines [1]. This paper focuses on twin-entry radial turbine applications where the inlet flows are not the same. This is the case for turbochargers of multi-cylinder engines. Usually, in these turbochargers, twin-entry radial turbines give the advantage of using the exhaust pulse energy of gases. In these applications, turbines often work under off-design conditions. Therefore, turbine performance characteristics under such conditions are important [1,2]. There are a few published studies of twin-entry radial turbines under full and partial admission conditions; almost all of them are experimental [3-5]. Pischiger and Wunsche [2] studied the interaction between the inlet gas flows from the twin-entry turbines under steady conditions. They showed that unequal inlet conditions have a significant effect on the flow pattern and turbine performance. Furthermore, they considered the isentropic flow area through each entry, and showed that this area depends on the pressure ratio between entries and the overall mean expansion ratio. The performance characteristics of a twin entry turbine were prepared experimentally by Dale and Watson [5], showing that the best efficiency is not under full admission conditions. Then, Capabianco and Gambarotta [6] showed experimentally the effect of each entry of the volute on full and partial admission conditions. Baines and Yeo [7] performed flow laser measurements in a turbine rotor inlet and exit under full and partial admission conditions. They suggested that the changes in performance under partial admission considerations are linked to a spanwise variation in the rotor incidence angle and velocity components at the rotor inlet.

The major modeling activities and performance predictions of a radial inflow gas turbine were focused on single entry turbines [8-12]. Chen and Winterbone modeled a single entry radial turbine [9]. Heribernik and Dobovisek [10] presented a model for predicting single and twin-entry turbine performances based on ideal relations. Gassemi et al. [12] presented a model for predicting single and twin entry turbine performances. They modified the one-dimensional performance prediction method of a single-entry turbine to analyze the twin-entry turbine performance.

1. *Department of Mechanical Engineering, Sharif University of Technology, Tehran, P.O. Box 11155-8639, Iran.*
*. *Corresponding author. E-mail: hajilouy@sharif.edu*

Received 24 February 2007; received in revised form 14 August 2007; accepted 10 February 2008

This research is based on experimental results. Due to the non-ideal measurement conditions, which were typically encountered during the test, the uncertainty of the test data is considered. A number of research findings and standard codes have discussed gas turbine testing errors and uncertainties [14]. The test codes of PTC10 [15], PTC 19.1 [16] discuss instruments, thermodynamic calculations and laboratory preparations. Dale and Watson [5] discussed the uncertainty of a radial inflow gas turbine and showed the variation of uncertainty with the speed ratio. Meanwhile, Yong and Penz [17] and Arcoumanis [18] presented a turbocharger test facility, test design and test procedure.

This paper describes a method of prediction of the performance of a twin-entry radial inflow turbine under steady, full and partial admission conditions. This model is based on one-dimensional performance prediction. Loss coefficients due to friction, clearance, blade loading and exit kinetic energy, which were already developed for a single entry turbine, are modified for a twin-entry turbine. Furthermore, additional losses are considered due to partial admission conditions. The results of the model are evaluated with experimental results. Finally, an analytic method is described to determine turbocharger turbine measurement uncertainties. By introducing experimental errors to the uncertainty equation, the efficiency uncertainties of the turbine are obtained.

MODELING

The steady state performance prediction model developed in this investigation is based on the solution of an adiabatic, steady state, one-dimensional flow in a twin-entry radial inflow turbine. In one-dimensional modeling, due to the three-dimensionality and complexity of the flow pattern within the turbine, a good understanding of the flow behavior is necessary to estimate accurate loss coefficients. In this method, the mean flow parameters are obtained along a mean streamline on key stations (inlet and exit of each section), using continuity, momentum, energy and state equations and the second law of thermodynamics. In this study, the turbine flow passage is divided into five components including inlet passage, volute casing, interspace, incidence and rotor which are shown in Figure 1, and the flow is modeled in each section with imposing loss equations. This model is implied for a turbine with the main geometrical dimensions as shown in Table 1.

Inlet Passage

The program input consists of turbine geometry, inlet total pressure and temperature and rotor speed, by

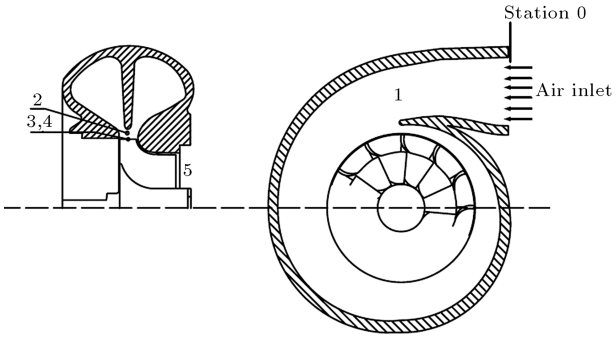

Figure 1. Twin-entry radial inflow gas turbine and main modeling stations.

Table 1. The turbine geometry.

Volute inlet area (A_0)	0.0022 (m^2)
Rotor inlet mean diameter (D_3)	0.0736 (m)
Rotor inlet blade height (b_3)	0.0088 (m)
Exducer hub diameter (D_{5h})	0.0233 (m)
Exducer shroud diameter (D_5s)	0.0576 (m)
Number of blades (Z)	11

assuming a range of the critical velocity ratio (C/C_{cr}) for each inlet (shroud side and hub side).Therefore, for this modeling, the critical velocity at each side is determined by [9]:

$$C_{cr} = \sqrt{\frac{2\gamma RT_{00}}{\gamma + 1}}. \tag{1}$$

Static density at the inlet is determined by:

$$\frac{\rho_0}{\rho_{00}} = \left[1 - \frac{\gamma - 1}{\gamma + 1}\left(\frac{C}{C_{cr}}\right)^2\right]^{1/\gamma - 1}. \tag{2}$$

Thus, the mass flow rate at the inlet of a turbine for each side is determined. The Mach number at station 1, Figure 1, (M_1) for each side is computed from the following equation, derived in [3]:

$$\frac{\dot{m}\sqrt{RT_{00}/\gamma}}{A_1 P_{00}} = \sigma_{0-1}\cos(\alpha_1) M_1 \left(1 + \frac{\gamma - 1}{2} M_1^2\right)^{\frac{\gamma+1}{2(1-\gamma)}}, \tag{3}$$

where:

$$\sigma = e^{(-\Delta s/R)}. \tag{4}$$

The inlet duct is short and direct. Therefore, its loss coefficient, σ_{0-1}, and exit flow angle, $\alpha 1$, are assumed one and zero, respectively. Having solved Equation 3, the flow properties in station 1, Figure 1, are determined.

Volute Casing

The turbine spiral volute exit flow parameters should be determined. In station 2, Figure 1, for each entry the following equation is computed iteratively:

$$\frac{\dot{m}\sqrt{RT_{01}/\gamma}}{A_2 P_{01}} = \sigma_{1-2}\cos(\alpha_2) M_2 \left(1+\frac{\gamma-1}{2}M_2^2\right)^{\frac{\gamma+1}{2(1-\gamma)}}. \quad (5)$$

The flow angle, α_2, and the flow entropy gain, σ_{1-2}, are obtained from a method presented by Balje [20]. Then, the iteration loop is repeated until the desired accuracy is obtained and exit Mach number and properties are determined.

Interspace

In the interspace area (stations 2 and 3, Figure 1), the interaction of the hub and the shroud side flows are taken into consideration (Figure 2). For determining the flow properties at the exit of this region, governing equations for each side are solved. The loss coefficient in this region is due to the friction of the hub and shroud streams and the wake of the divider. The method used to calculate the wake loss is given in [21].

The friction and the wake losses are calculated separately. Friction loss and flow angle are obtained using a simple numerical method to solve continuity, momentum, energy and gas state equations simultaneously. The wake loss is obtained by considering the average condition in the inlet and the simultaneous solving of the governing equations [21]; half of the wake loss is considered for each entry. Then, these two losses are added together for each entry. Therefore, $\sigma_{2-3,\text{friction}}$ and $\sigma_{2-3,\text{wake}}$ are defined, and the following total flow entropy gain correlation for each entry is used to calculate the losses in the interspace area:

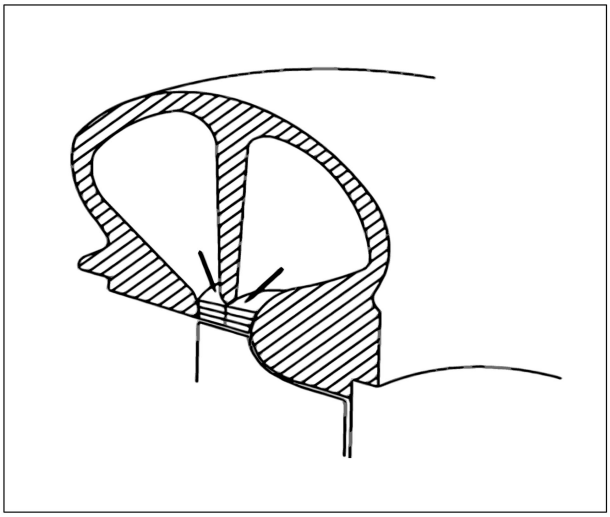

Figure 2. Hub and shroud velocity.

$$\sigma_{2-3} = \sigma_{2-3,\text{friction}} \cdot \sqrt{\sigma_{2-3,\text{wake}}}. \quad (6)$$

In section 3, Figure 1, for each entry Equation 6 is solved iteratively:

$$\frac{\dot{m}\sqrt{RT_{02}/\gamma}}{A_3 P_{02}} = \sigma_{2-3}\cos(\alpha_3) M_3 \left(1+\frac{\gamma-1}{2}M_3^2\right)^{\frac{\gamma+1}{2(1-\gamma)}}. \quad (7)$$

Incidence

Incidence loss at the rotor inlet is the main cause of an efficiency drop under off-design conditions. In practice, the best efficiency occurs at an optimum incidence angle. Therefore, any deviation from the optimum incidence angle causes extra losses. In this modeling, the incidence area (stations 3 and 4, Figure 1) is a hypothetical region and the incidence loss is part of the rotor loss, but for the reason of modeling strategy it is modeled separately. The objective of the incidence model is to drive an entropy increase due to the incidence angle. Several models have been introduced to calculate the incidence losses. In this study, a NASA extended model is used, which is based on the assumption that the kinetic energy associated with the change in relative tangential velocity is converted into the internal energy of the working fluid [9]. This region is assumed as a moving passage and Equation 8 is used for computing the relative Mach number at this section:

$$\frac{\dot{m}\sqrt{RT'_{03}/\gamma}}{P'_{03}A_4} = \sigma_{3-4} M'_4 \left(1+\frac{\gamma-1}{2}M'^2_4\right)^{-(\gamma+1)/2(\gamma-1)}. \quad (8)$$

The incident loss, σ_{3-4}, is calculated by [10]:

If $|\beta_3 - \beta_{3opt}| > \pi/4$ then :

$$\Delta h'_{0inc} = h'_{03} - h'_{04s} = \frac{1}{2}\left[W_3 \sin\left(|\beta_3 - \beta_{3opt}|\right)\right]^2. \quad (9)$$

And if $|\beta_3 - \beta_{3opt}| < \pi/4$, then:

$$\Delta h'_{0inc} = \frac{1}{2}W_3^2\left(0.5 + |\beta_3 - \beta_{3opt}| - \pi/4\right). \quad (10)$$

So:

$$\sigma_{3-4} = \left(1 - \frac{\Delta h'_{0inc}}{c_p T'_{03}}\right)^{\frac{\gamma}{\gamma-1}}. \quad (11)$$

Also, the optimum flow angle is calculated by [3]:

$$\beta_{3opt} = \arctan\left(\frac{-1.98}{Z_B(1-1.98/Z_B)}\tan(\alpha_3)\right). \quad (12)$$

Rotor

The complex three-dimensional flow pattern in the rotor raises the difficulties in the rotor modeling and causes major turbine losses in the rotor. The following equations are used for flow modeling at the single-entry turbine rotor, which combines the equations of continuity, energy and entropy [3]:

$$\frac{\dot{m}\sqrt{RT'_{04}/\gamma}}{A_5 P'_{04}} = \cos(\beta_5).\sigma.M'_5 \left(1+\frac{(\gamma-1)}{2}M_5'^2\right)^{-(\gamma+1)/2(\gamma-1)} \left(1-\frac{U_4^2-U_5^2}{2c_pT'_{04}}\right)^{(\gamma+1)/2(\gamma-1)}, \quad (13)$$

where:

$$\sigma = \left(1-\frac{\gamma-1}{\gamma RT'_{0e}}U_t^2\Delta q\right)^{\gamma/(\gamma-1)}, \quad (14)$$

$$\Delta q = \frac{h'_{0e}-h'_{0es}}{U_t^2} = \frac{\Delta h'_{0es}}{U_t^2}. \quad (15)$$

Equation 13 is modified for the twin-entry turbine rotor, considering the effect of partial admission conditions. Therefore, the following non-dimensional equation is used for modeling the twin-entry rotor flow area (stations 4 and 5, Figure 1) [13]:

$$\frac{\dot{m}\sqrt{R/\gamma}}{A_5}\left(\frac{\sqrt{T'_{04,s}}}{P'_{04,s}}\right)^{Mr_s}.\left(\frac{\sqrt{T'_{04,h}}}{P'_{04,h}}\right)^{Mr_h} = \sigma_{4-5}.\cos(\beta_5)M'_5\left(1+\frac{(\gamma-1)}{2}M_5'^2\right)^{-\frac{(\gamma+1)}{2(\gamma-1)}} \left\{\left(1-\frac{U_4^2-U_5^2}{2C_pT'_{04,s}}\right)^{Mr_s} .\left(1-\frac{U_4^2-U_5^2}{2C_pT'_{04,h}}\right)^{Mr_h}\right\}^{\frac{(\gamma+1)}{2(\gamma-1)}}, \quad (16)$$

where $Mr_s = \frac{\dot{m}}{\dot{m}_s+\dot{m}_h}$ and $Mr_h = \frac{\dot{m}_h}{\dot{m}_s+\dot{m}_h}$.

In Equation 16, the effect of shroud and hub side flow losses can be considered. For this reason, the following model is suggested [13]:

$$\sigma_{4-5} = \left\{\left(1-\frac{\gamma-1}{\gamma RT'_{05}}U_t^2\Delta q_s\right)^{Mr_s} \left(1-\frac{\gamma-1}{\gamma RT'_{05}}U_t^2\Delta q_h\right)^{Mr_h}\right\}^{\frac{\gamma}{\gamma-1}}. \quad (17)$$

Also, the single-entry rotor loss coefficient is modified to obtain losses in the twin-entry rotor as follows.

a) Friction Loss

This loss is computed in the same way as obtained in a curved duct [11,22]:

$$\Delta q_{fr} = f_c\frac{L_H}{D_H}.\frac{\bar{W}^2}{2U_t^2}, \quad (18)$$

$$\bar{W}^2 = \frac{1}{2}\left[(Mr_sW_{4s}+Mr_hW_{4h})^2+W_5^2\right], \quad (19)$$

$$f_c = f(1+0.75Re^{0.25}\sqrt{D_H/2r_c}), \quad (20)$$

where:

$$\frac{1}{\sqrt{f}} = 0.2\ln\left(Re_{D_H}\sqrt{f}\right)-1.19. \quad (21)$$

b) Blade Loading Loss

The following equation is used to calculate the blade loading loss [23]:

$$\Delta q_{bl} = \frac{C_{\theta 3}^2 D_t}{ZL_RU_t^2}. \quad (22)$$

L_R is calculated using the equation given by Whitfield and Baines [3].

c) Clearance Loss

The clearance loss is calculated from the following equation [3]:

$$\Delta q_{cl} = 0.4(e_{Cl}/b_t)(C_{\theta 3}/U_t)^2, \quad (23)$$

where:

$$e_{Cl} = 0.008/(2b_t/D_t). \quad (24)$$

d) Exit Loss

The exit loss is considered with the assumption that the kinetic energy associated with rotor exit velocity, at the outlet of the rotor, is dissipated:

$$\Delta q_{\text{exit}} = 0.5\frac{C_5^2}{U_t^2}. \quad (25)$$

Finally, the non-dimensional energy loss in the rotor Δq_{total} is determined:

$$\Delta q_{\text{total}} = \Delta q_{fr} + \Delta q_{bl} + \Delta q_{cl} + \Delta q_{\text{exit}}, \tag{26}$$

$$\sigma_R = e^{(-\Delta s/R)} = \left(1 - \frac{\gamma - 1}{\gamma R T'_{05}} U_t^2 \Delta q_{\text{total}}\right)^{\gamma/(\gamma-1)}. \tag{27}$$

e) Rotor Mixing Loss

Rotor mixing loss is considered only in the twin-entry radial turbine, as a result of the difference in the mass flows of the shroud and hub entries. As shown in Figure 3, the entropy increase for this process can be obtained by solving the governing equation within the control volume, encompassing the mixing process at the rotor inlet for revealing the downstream flow properties and the entropy gain. Therefore, the entropy gain associated with the mixing process between hub and shroud side flows is obtained from:

$$\frac{\Delta s_m}{R} = \frac{\gamma}{\gamma - 1} \ln\left(\frac{T_y}{\bar{T}_3}\right) - \ln\left(\frac{P_y}{\bar{P}_3}\right), \tag{28}$$

$$\sigma_{R-\text{mixing}} = e^{(-\Delta s_m/R)}. \tag{29}$$

Finally, the rotor loss coefficient is obtained:

$$\sigma_{\text{rotor}} = \sigma_{4-5} = \sigma_R . \sigma_{R-\text{mixing}}. \tag{30}$$

SOLUTION PROCEDURE

The analysis consists of a section by section solution of flow conditions through the turbine along the mean streamline. In this procedure, the turbine geomety is specified. Meanwhile, at a fixed rotor speed, speed velocity ratios for both entries are given. With this ratio, the mass flow for each entry is specified. Under these conditions, flow equations for each section are solved up to the end. The iteration loop is repeated until the desired accuracy is reached. By solving the flow equations, the Mach number, loss coefficent and exit properties for each area are determined. Thus, at the end of each area, exit conditions, which are inlet conditions of the next area, are determined. In this procedure, flow at each side is considered separately up to passage 4-5. In passage 4-5, just one flow is considered. At the end of the procedure, the mass parameter, pressure ratio and total-static efficiency are calculated and this procedure is repeated for the next velocity ratio up to the end of the (C/C_{cr}) range. Indeed, in this program, the stator is chocked when $(C/C_{cr})_3 = 1$ and the rotor is chocked when $(W/W_{cr})_5 = 1$, which are the maximum flows per unit area, and the program is terminated at these conditions.

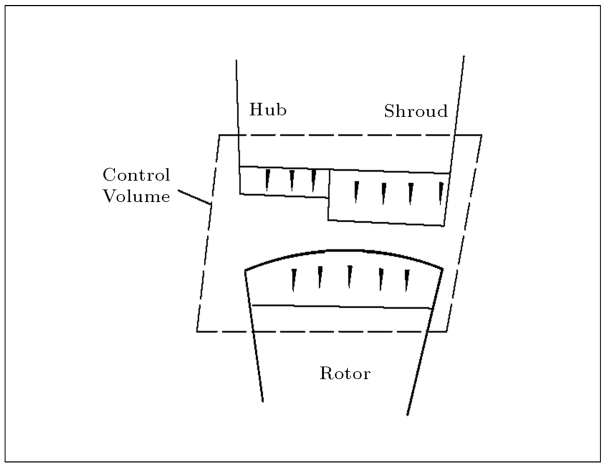

Figure 3. Hub and shroud mixing station.

TURBOCHARGER LABORATORY

The turbocharger test rig has been designed, established and equipped to investigate different automotive turbochargers under a variety of operational conditions, based on the flow simulation of a turbocharger using compressed air. The main specifications of the test, which can be carried out in the rig, are as follows:

1. Steady flow tests using a compressor to absorb and measure the power of the turbine;
2. Full and partial admission measurements on a twin-entry turbine using a twin-inlet test system. The arrangement of the test rig facility is shown schematically in Figure 4.

Three screw compressors are employed to produce high pressure air, adjustable up to a 13 bar gauge with a mass flow rate of 0.4 kg per sec. The main compressed air supply line is a 3-inch diameter pipe. The mass flow rate is adjusted using an electro-pneumatic valve. In order to measure the steady flow air mass flow rate, in turbine side three and in the compressor side, one orifice plate calibrated to BS 1042 is used [19]. The compressed air can be heated up to 200 degrees Celsius using an electrical heater unit. This is to prevent the condensation of any water vapor at the turbine blades, where there is a high temperature drop due to the air expansion. The heater unit consists of 32 elements, each 2 kW in power, suitable for various mass flow rates and different temperature rise conditions. A turbocharger compressor absorbs the turbine output power, acting as a dynamometer, and controls the rotational speed of the turbocharger. The compressor outlet air passes through an additional throttle valve and is exhausted to the atmosphere out of the laboratory by a two-inch exit duct. Also, the mass flow rates to the two-entry can be controlled independently. A

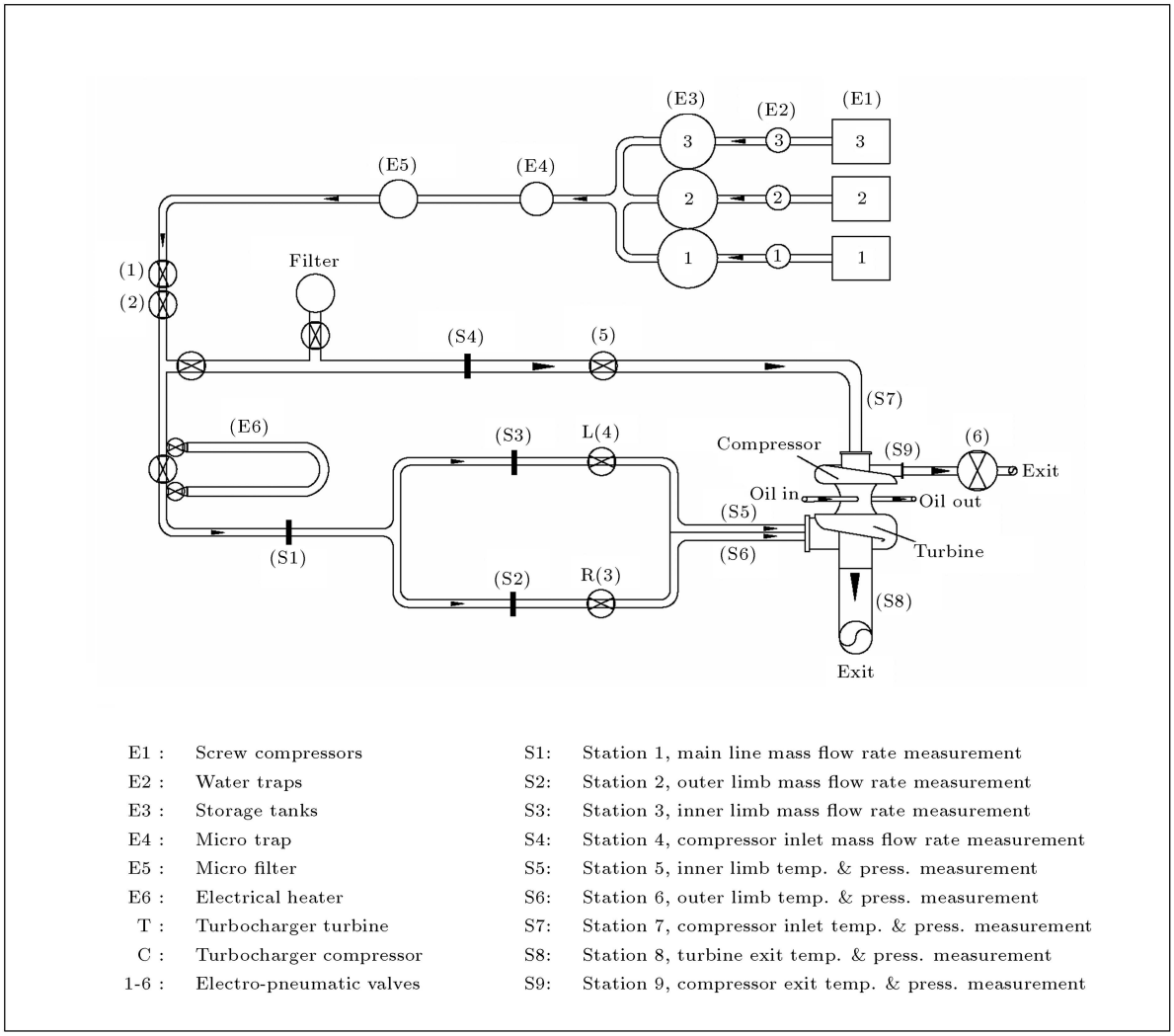

Figure 4. Schematic of turbocharger test rig and measuring stations.

full admission condition to the turbine occurs when the control valves of each entry are fully opened. A partial admission flow condition is achieved by varying the flow in each entry. The full admission performance of a twin-entry turbine for 30000, 40000, 50000 and 60000 rpm is shown in Figures 5 and 6. The operation range is limited by the surge point of the loading compressor. Figure 5 shows the mass flow curves and Figure 6 shows the total-static efficiency curves versus the pressure ratio. The maximum difference between experimental and theoretical results under full admission conditions is 2% for mass parameter and 1.5% for efficiency.

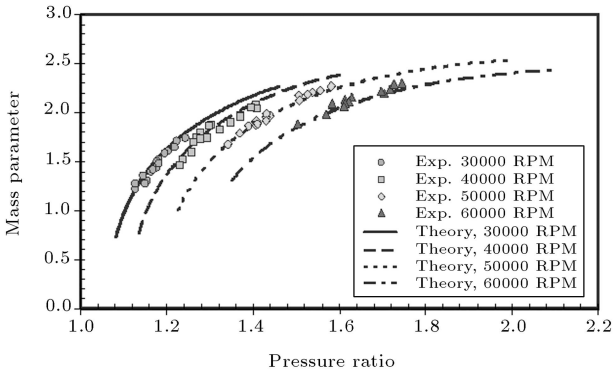

Figure 5. Experimental and theoretical results of mass flow characteristics under full admission.

FULL AND PARTIAL ADMISSION RESULTS

In the literature, Zanghaneh et al. [24] for a single-entry turbine, and Baines and Yeo [7] for a twin-entry turbine with full and partial admission conditions showed that the flow at the rotor inlet tends to pass through the shroud side, and the best efficiency is obtained when there is more flow in the shroud side. As shown in experimental results (Figure 7), the best efficiency occurs when $M_s/M_h = 1.15$. Therefore, in this case, losses are the lowest. Figure 8 shows that in

this condition, the mass flow parameter is higher than the full admission condition with the same pressure ratio due to lower losses. Figure 9 shows the efficiency prediction of the turbine under five different partial admission conditions that are compared with experimental results at 50000 rpm, having the maximum

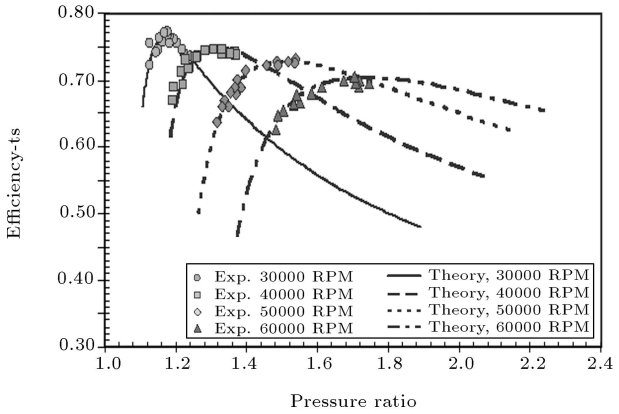

Figure 6. Experimental and theoretical results of efficiency characteristics under full admission.

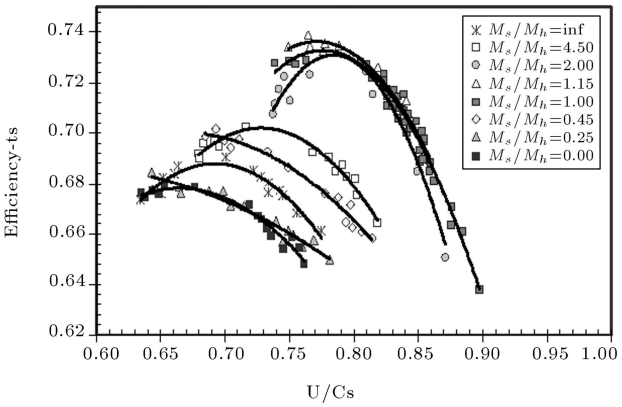

Figure 7. Measured efficiency under full and partial admission at 50000 rpm.

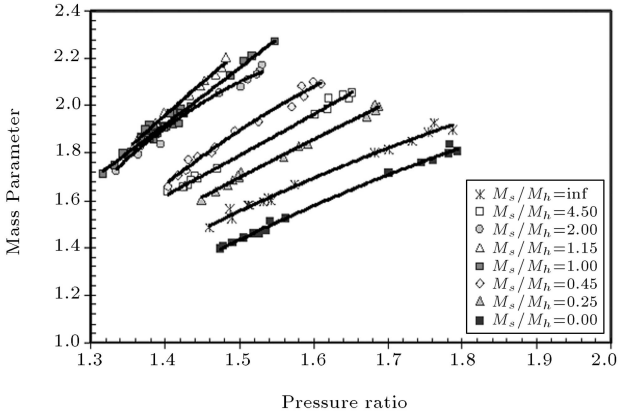

Figure 8. Measured mass parameter under full and partial admission at 50000 rpm.

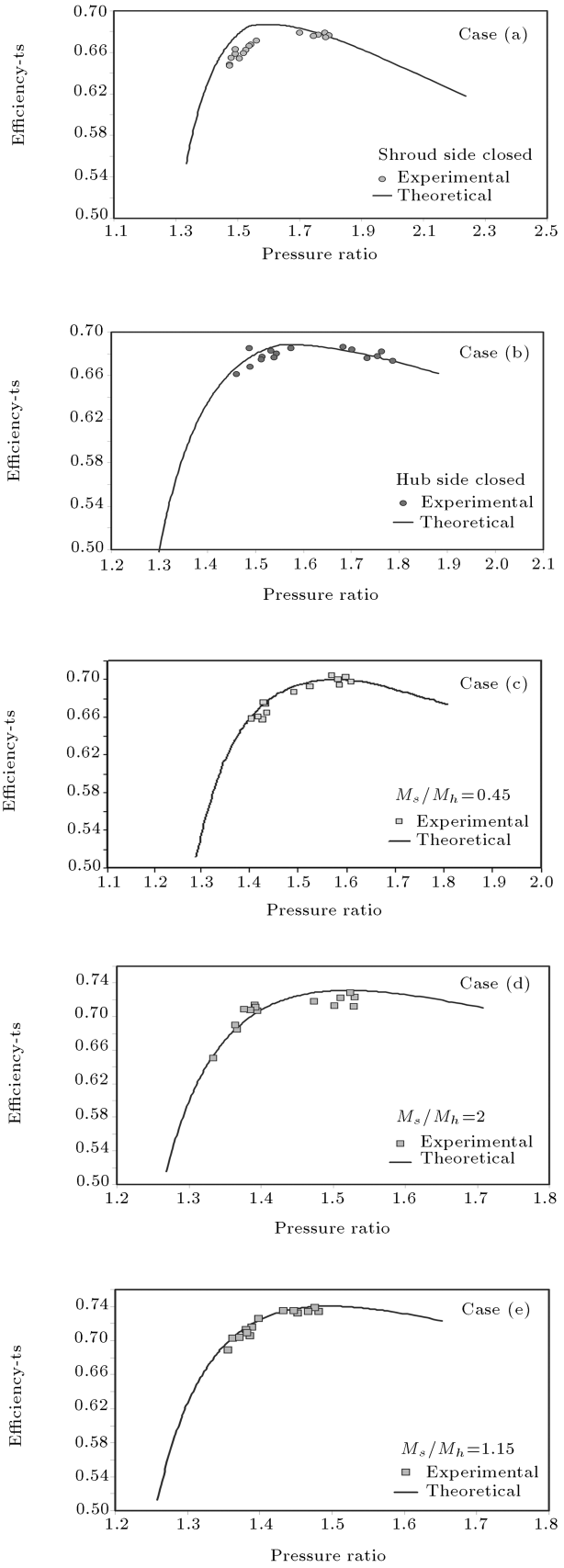

Figure 9. Experimental and modeling efficiency results under partial admission at 50000 rpm.

deviation of calculated results from experimental data for a shroud side closed condition (Case a). This can be due to the less accurate estimate of the mixing loss at the inlet of the rotor.

TURBINE TEST UNCERTAINTIES

After calibrating the instruments, making sure of correct installation and conforming to standard codes, the sources of measurement errors encountered during test measurements should be determined. Measurements are always subject to error, i.e. the difference between the true and measured values. Since the true value is unknown, the error in measurement cannot be determined exactly. Therefore, only the error band can be estimated. Thus, uncertainty is introduced, which is an estimate of the interval about the measurement value that is expected to encompass the true value.

The total measurement error consists of two components: (1) Systematic error or bias or fixed error; (2) Random error. Accurate measurement requires minimization of both systematic and random errors [16].

For uncertainty analysis, a procedure is introduced that consists of five basic steps, as explained in detail in [25].

Data Reduction Equations

The total to static efficiency equation of a turbine is as follows:

$$\eta_{ts} = \frac{1 - \frac{T_{0\text{out}}}{T_{0\text{in}}}}{1 - \left[\frac{P_{\text{out}}}{P_{0\text{in}}}\right]^{\frac{\gamma-1}{\gamma}}}. \tag{31}$$

Therefore, the parameters that are measured during a test for this case are: the turbine inlet and outlet temperatures and pressures.

Sensitivity Coefficients

Sensitivity coefficients play an important role in evaluating instrument errors, also helping to identify parameters which have the most significant effect on uncertainty. The sensitivity coefficient is the ratio of the change in the result to a unit change in parameters. The relative sensitivity of y to X_i is given by:

$$S_{r\bar{X}_i} = \left(\frac{\partial y}{\partial \bar{X}_i}\right)\left(\frac{\bar{X}_i}{y}\right). \tag{32}$$

Substituting Equation 31 into Equation 32 gives the relative sensitivity of efficiency to a unit change in each parameter of Equation 31. As shown in Table 2, the sensitivity of efficiency to the input and output temperature is more than the input and output pressure. Therefore, temperature has a stronger influence on efficiency. Meanwhile, as the pressure ratio increases, sensitivity to the pressure and temperature decreases.

Uncertainty of Results

For an uncertainty analysis, it is assumed that all measurement parameters are independent and have Gaussian normal distributions around their mean values with a statistical bound of a 95% confidence interval. So, total uncertainty, U_{95}, for a given function, X, is determined as:

$$B_{ry} = t_{95}\left[\sum_{i=1}^{j}\left(S_{r\bar{X}_i}\frac{\beta_{r\bar{X}_i}}{2}\right)^2\right]^{1/2}, \tag{33}$$

$$\sigma_{ry} = \left[\sum_{i=1}^{j}(S_{r\bar{X}_i}\sigma_{r\bar{X}_i})^2\right]^{1/2}, \tag{34}$$

$$U_{r95} = t_{95}\sqrt{\left(\frac{B_{ry}}{2}\right)^2 + (\sigma_{ry})^2}. \tag{35}$$

In these equations, t_{95} is determined by student-t distribution.

The total uncertainty of the turbine efficiency versus pressure ratio for four test speeds is shown in Figure 10. As the pressure ratio increases, the efficiency uncertainty decreases in the range of the experimental pressure ratio. In the range of the experimental pressure ratio, high uncertainty in the low pressure ratio shows a higher sensitivity of uncertainty to the low speed condition in the turbine. This result is expected and can be explained as follows: The larger the pressure or temperature inlet-outlet differential, the smaller the relative influence of individual measurement errors on total performance uncertainties.

Table 2. Mean relative sensitivity of efficiency in constant speed at 50000 rpm.

Pressure Ratio	Exit Pressure (%)	Inlet Pressure (%)	Exit Temperature (%)	Inlet Temperature (%)
1.372	2.98	-2.98	-15.36	15.36
1.387	2.91	-2.91	-14.86	14.86
1.398	2.84	-2.84	-14.47	14.47
1.412	2.75	-2.75	-13.83	13.83
1.425	2.69	-2.69	-13.50	13.50

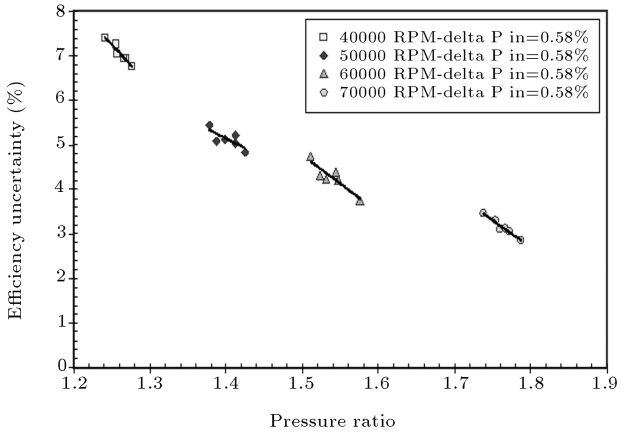

Figure 10. Total efficiency uncertainty versus turbine pressure ratio.

CONCLUSION

In this paper, a one-dimensional flow model for the performance prediction of a twin-entry radial inflow gas turbine under partial and full admission conditions is presented. A steady flow model, based on loss correlation, is used to predict the turbine performance. Results of this model are compared with experimental data and they are in reasonable agreement. The main limitation in experimental data is due to the compressor surge. The difference between experimental and theoretical results under full admission conditions is 2% for mass parameter and 1.5% for efficiency. However, under partial admission conditions, the maximum difference between results reaches to 5% for a shroud side closed case and this deviation can be due to a less accurate estimate of mixing loss and equally divided interspace loss. Also, the total uncertainty of the turbine efficiency is obtained and results show that it decreases as the pressure ratio increases. Also, the high uncertainty in the low pressure ratio illustrates turbine sensitivity to the low speed condition.

ACKNOWLEDGMENTS

The authors gratefully acknowledge the valuable support and funding of the Energy Conversion Center at Sharif University of Technology, as well as the Ministry of Industry of I.R. IRAN.

NOMENCLATURE

A	area
b	blade height
D	diameter
e	clearance between rotor blades and shroud
f	skin friction coefficient for smooth wall
f_c	skin friction coefficient for curved pipe
L	length
M	mass flow rate, Mach number
Mr_h	hub side entry mass flow rate to total mass flow rate
Mr_s	shroud side entry mass flow rate to total mass flow rate
P	pressure
Re	Reynolds number
T	temperature
C	flow velocity
U	blade velocity
Z	rotor blade number
β	relative angle of flow
η	efficiency
σ	loss coefficient
s	entropy, sensitivity coefficient
$U(y)$	uncertainty
$\bar{P}$	mass average pressure
$\bar{T}$	mass average temperature

Subscripts and Superscripts

0	turbine entry, stagnation property
1	volute casing entry
2	interspace entry
3	rotor entry
4	inlet to rotor
5	rotor exit
BL	blade loading
Cl	clearance
y	passage exit (downstream of rotor inlet)
h	hub side
s	shroud side
ts	total to static
R	rotor
fr	friction
H	hydraulic
m	mixing
$'$	relative condition

REFERENCES

1. Watson, N. and Janota, M.S. "Turbocharging the internal combustion engine", *Longman Scientific and Technical Publishing Company* (1982).
2. Pischinger, F. and Wunsche, A. "The characteristic behavior of radial turbines and its influence on the turbocharging process", *12th International Congress on Combustion Engines*, CIMAC, Tokyo (1977).

3. Whitfield, A. and Baines, N.C., *Design of Radial Turbomachines*, Longman Scientific and Technical Publishing Company (1990).
4. Hajilouy, A. and Baines, N.C. "Twin-entry radial turbine flow measurements under unsteady flow conditions", *4th Conference of ISME*, pp. 233-244 (1996).
5. Dale, A. and Watson, N. "Vaneless radial turbocharger turbine performance", *IMechE*, **C110/86**, pp. 65-76 (1986).
6. Capobianco, M. and Gambarotta, A. "Performance of a twin-entry automotive turbocharger turbine", *ASME Paper*, **93-ICE-2** (1993).
7. Baines, N.C. and Yeo, J.H. "Flow in a radial turbine under equal and partial admission conditions", *IMechE*, **C423/002**, pp. 103-112 (1991).
8. Miyauchi, A. and Yoshiki, H. "One-dimensional passage modeling of a radial turbine on the basis of design specifications", *IMechE*, **C484/033/94**, pp. 265-270 (1994).
9. Chen, H. and Winterbone, D. E. "A method to predict performance of vaneless radial turbines under steady and unsteady flow conditions", *IMechE*, **C405/008**, pp. 13-22 (1990).
10. Heribernik, A. and Dobovisek, Z. "Application of rotor characteristics for one-dimensional turbine modeling", *IMechE*, **C484/034/94**, pp. 38-47 (1994).
11. Abidat, M. and Baines, N.C. "Prediction of steady and non-steady flow performance of highly loaded mixed flow turbine", *Proc. IMechE*, **212**(A), pp. 173-183 (1998).
12. Connor, W.A. and Flaxington, D.A. "One-dimensional performance prediction method for radial inflow turbines", *IMechE*, **C484/041/94**, pp. 271-281 (1994).
13. Ghasemi, S., Shirani, E. and Hajilouy-Benisi, A. "Performance prediction of twin-entry turbocharger turbines", *ASME TURBO EXPO Conference*, **GT-2002-30576**, pp. 1-9 (2002).
14. Nakra, B.C., *Instrumentation Measurement and Analysis*, Tata- McGraw-Hill (1991).
15. ASME PTC 10 "Compressor and exhausters" (1994).
16. ASME PTC 19.1 "Performance test code on compressor and exhausters" (2005).
17. Young, M.Y. and Penz, D.A. "The design of a new turbocharger test facility", *SAE*, **900176**, pp. 873-885, (1990).
18. Arcoumanis, C., Karamanis, N. and Martinez, R.F. "Unsteady characteristics of a mixed flow turbocharger turbine", *IMechE*, **C557/030/99**, pp. 905-922 (1999).
19. BS-1042, "Method of measurement of fluid flow in closed conduits" (1981).
20. Balje, O.E., *Turbomachines: A Guide to Design Selection and Theory*, John Wiley & Sons, New York (1981).
21. Rose, M.G. and Harvey, N.W. "Turbomachinery wakes: Differential work and mixing losses", *Transaction of the ASME, Journal of Turbomachinery*, **212**, pp. 68-77 (2000).
22. Schlichting, H. translated by Kestin, J., *Boundary-Layer Theory*, Sixth Ed., McGraw-Hill Book Company (1968).
23. Rodgers, C. "Mainline performance prediction on radial inflow turbines", *VKI Lecture Series*, **1987-07**, pp. 1-30 (1987).
24. Zanganeh-Kazemi, M., Dawes, W.N. and Hawthorne, R. "Three-dimensional flow in radial inflow turbines", *ASME Paper*, **88-GT-103**, pp. 1-9 (1988).
25. Rad, M., Hajilouy, A. and Shahhosseini, M.R. "Evaluation of empirical performance characteristics of turbocharger turbine and compressor", *9th AIAA/ASME Joint Thermophysics and Heat Transfer Conference* (2006).